

Banner appropriate to article type will appear here in typeset article

How far does turbulence spread?

Alexandros Alexakis¹†,

¹Laboratoire de Physique de l'Ecole Normale Supérieure, ENS, Université PSL, CNRS, Sorbonne Université, Université de Paris, F-75005 Paris, France

(Received xx; revised xx; accepted xx)

How locally injected turbulence, spreads in space is investigated with direct numerical simulations. We consider a turbulent flow in a long channel generated by a forcing that is localised in space. The forcing is such that it does not inject any mean momentum in the flow. We show that at long times a statistically stationary state is reached where the turbulent energy density in space fluctuates around a mean profile that peaks at the forcing location and decreases fast away from it. We measure this profile as a function of the distance from the forcing region for different values of the Reynolds number. It is shown, that as the Reynolds number is increased, it converges to a Reynolds-independent profile implying that turbulence spreads due to self-advection and not molecular diffusion. In this limit therefore, turbulence plays the simultaneous role of cascading the energy to smaller scales and transporting it to larger distances. The two effects are shown to be of the same order of magnitude. Thus a new turbulent state is reached where turbulent transport and turbulent cascade are equally important and control its properties.

1. Introduction

A drop of dye in a fluid will spread so that at long times it is uniformly distributed in the entire space. This is not necessarily true for a turbulent puff introduced locally in an otherwise still fluid. Turbulent energy will also spread either by viscous diffusion or by self-advection but at the same time will dissipate. *At long times, if constantly injected, will the spreading of turbulence be able overcome the dissipation so that turbulence spreads throughout the domain or dissipation will limit its presence only near its source?* The answer to this question is not *a priori* obvious and is fundamental for understanding inhomogeneous turbulent flows.

Inhomogeneous flows have been the subject of various recent studies (Valente & Vassilicos 2011; Gomes-Fernandes *et al.* 2015; Alves-Portela *et al.* 2020; Araki & Bos 2022; Berti *et al.* 2023) that have all emphasised the effect of inhomogeneity in the cascade process which can make it deviate from the classical homogeneous case. In particular it has been shown that inhomogeneity can alter the scale by scale balance of the cascade (Apostolidis *et al.* 2022, 2023) and change its scaling properties. Furthermore, inhomogeneity is an indispensable ingredient of many classical canonical flows such as the spreading of a turbulent jet (List 1982; Carazzo *et al.* 2006; Ball *et al.* 2012; Cafiero & Vassilicos 2019) and the spreading of turbulence from the boundaries in wall bounded flows (Jiménez 2012; Gomes-Fernandes *et al.* 2015; Cimarelli *et al.* 2016; Mollicone *et al.* 2018). In these cases however along with the injection of energy there is also a mean injection of momentum. Momentum, unlike

† Email address for correspondence: alexakis@phys.ens.fr

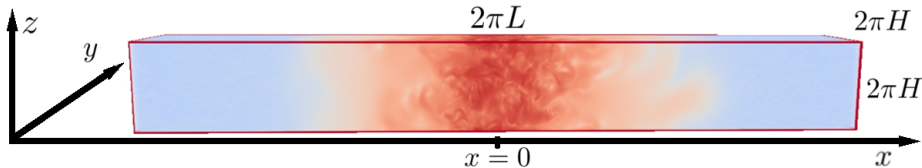


Figure 1: The computational domain considered. The length L was chosen to be eight times the height $L = 8H$ and $x = 0$ is taken to be at the middle of the channel. The colors indicate visualisations of the enstrophy $(\nabla \times \mathbf{u})^2$ with red indicating high values while blue are small values.

energy, is not dissipated by viscosity and it can only be transferred in space (by viscosity or advection) or out of the domain through the boundaries by viscous forces. Thus, much like the example of the drop of dye, the injected momentum will spread through out the space carrying along energy. The same holds if the injected energy has a mean angular-momentum that is also conserved by viscous forces. Therefore, in the case that there is mean momentum injection the answer to the question posed in the first paragraph is that momentum and energy will occupy the entire domain. The present work investigates the spreading of turbulence in the absence of mean momentum and angular momentum injection which is fundamentally different from the cases mentioned before.

To do that we consider turbulence generated in a long triple-periodic channel. The flow is forced homogeneously in the two short directions of the channel and locally in the long direction. The forcing is such that no mean momentum is injected. We study the behavior of the flow inside and outside the forcing region at long times, measuring the energy distribution and energy fluxes in real and spectral space. In the next section 2 we present the mathematical set up of the system under study and define all relative quantities under investigation. In section 3 we present the results from numerical simulations. Conclusions are drawn in the final section 4 where directions for future research are also discussed.

2. Formulation

2.1. Mathematical setup

A triple periodic domain of size $2\pi L \times 2\pi H \times 2\pi H$ is considered as shown in figure 1 with $L \gg H$ being along the x -direction and $x = 0$ is taken to be the mid-plane of the channel. The flow inside the domain satisfies the Navier-Stokes equation

$$\partial_t \mathbf{u} + \mathbf{u} \cdot \nabla \mathbf{u} = -\nabla P + \nu \nabla^2 \mathbf{u} + \mathbf{f} \quad (2.1)$$

where \mathbf{u} is the divergence free velocity field ($\nabla \cdot \mathbf{u} = 0$), P is the pressure, ν is the viscosity and \mathbf{f} is the forcing. The functional form of the forcing is given by

$$\mathbf{f}(t, \mathbf{x}) = \begin{bmatrix} 0 \\ \partial_z [\psi(t, \mathbf{x}/\ell) - \psi(t, -\mathbf{x}/\ell)] \\ \partial_y [\psi(t, -\mathbf{x}/\ell) - \psi(t, \mathbf{x}/\ell)] \end{bmatrix} \exp \left[\frac{L^2}{\ell^2} \left(\cos \left(\frac{x}{L} \right) - 1 \right) \right] \quad (2.2)$$

where $\psi(t, \mathbf{x}/\ell)$ is a random function including only Fourier modes with wave-vectors \mathbf{k} satisfying $0 < |\mathbf{k}\ell| \leq 2$ and $k_x \neq 0$. The phases of these modes are delta correlated in time so that the mean energy injection rate is fixed to \bar{I}_0 . The forcing is anti-symmetric with respect to reflections in the $x = 0$ plane. As a result there is zero momentum injection for every realisation. Furthermore the forcing satisfies $\nabla \cdot \mathbf{f} = 0$. For $|x| \ll L$ the exponential factor to the right of 2.2 scales like $\exp(-x^2/\ell^2)$ so that the forcing is limited only around the range $|x| \sim \ell$ and zero outside. In the numerical simulations that follow we have picked

$\ell = H$ and $L = 8H$ that was proven (a posteriori) to be long enough so that the effect of the periodicity along the x direction does not play a role.

2.2. Energy balance relations and fluxes in space

The primary quantity of interest in this work is the time and volume averaged energy density of the system that is given by

$$\mathcal{E}_0 = \frac{1}{2} \left\langle \langle |\mathbf{u}|^2 \rangle_v \right\rangle_T \quad (2.3)$$

where the angular brackets $\langle \cdot \rangle_T$ stand for time average and $\langle \cdot \rangle_v$ for volume average defined as

$$\langle f \rangle_T = \lim_{T \rightarrow \infty} \frac{1}{T} \int_0^T f dt \quad \text{and} \quad \langle f \rangle_v = \frac{1}{V} \int_V f dx dy dz, \quad (2.4)$$

with $V = (2\pi)^3 H^2 L$ being the system volume. The averaged rate \mathcal{I}_0 that energy is injected is balanced by the averaged rate \mathcal{D}_0 that energy is dissipated, leading to

$$\mathcal{I}_0 \equiv \langle \langle \mathbf{u} \cdot \mathbf{f} \rangle_T \rangle_v = 2\nu \langle \langle |\mathbf{S}|^2 \rangle_T \rangle_v \equiv \mathcal{D}_0 \quad (2.5)$$

where \mathbf{S} stands for the strain tensor

$$S_{i,j} = \frac{1}{2} [\partial_i u_j + \partial_j u_i]. \quad (2.6)$$

However, neither the time averaged energy, nor its injection nor its dissipation are uniform along the x direction. It is thus appropriate to consider the mean energy density in a subdomain of the periodic box

$$\mathcal{E}(X) = \frac{1}{2} \left\langle \langle |\mathbf{u}|^2 \rangle_T \right\rangle_x \quad (2.7)$$

where $\langle \cdot \rangle_x$ stands for the average confined in the sub-box from $x = -X$ to $x = X$:

$$\langle f \rangle_x = \frac{1}{(2\pi H)^2} \int_0^{2\pi H} \int_0^{2\pi H} \int_{-X}^X \langle f(x, t) \rangle_T dx dy dz. \quad (2.8)$$

For $X = \pi L$ the entire box is considered so clearly $\mathcal{E}(\pi L) = 2\pi L \mathcal{E}_0$. We also define the local energy density averaged over the planes $x = \pm X$

$$E(t, X) = \frac{1}{2(2\pi H)^2} \int_0^{2\pi H} \int_0^{2\pi H} |\mathbf{u}(t, X, y, z)|^2 + |\mathbf{u}(t, -X, y, z)|^2 dy dz. \quad (2.9)$$

The two energy densities are related by $\langle E(X) \rangle_T = \partial_X \mathcal{E}(X)$.

A generalisation of eq. 2.5 for $\mathcal{E}(X)$ can then be obtained by taking the inner product of the Navier-Stokes equation with \mathbf{u} time averaging and integrating over y, z and from $x = -X$ to $x = X$ to obtain:

$$\mathcal{I}(X) = \mathcal{D}(X) + \mathcal{F}(X) \quad (2.10)$$

where $\mathcal{I}(X)$ and $\mathcal{D}(X)$ are the energy injection rate the energy dissipation rate within the considered volume defined respectively as:

$$\mathcal{I}(X) \equiv \langle \langle \mathbf{f}(t, \mathbf{x}) \cdot \mathbf{u}(t, \mathbf{x}) \rangle_X \rangle_T, \quad \text{and} \quad \mathcal{D}(X) \equiv 2\nu \langle \langle |\mathbf{S}(t, \mathbf{x})|^2 dx \rangle_X \rangle_T. \quad (2.11)$$

The third term $\mathcal{F}(x)$ is a flux that expresses the rate energy is transferred outside the considered volume (Landau & Lifshitz 2013). It can be decomposed in three terms

$$\mathcal{F} = \mathcal{F}_U + \mathcal{F}_P + \mathcal{F}_v \quad (2.12)$$

where \mathcal{F}_U is the energy flux due advection, \mathcal{F}_P the flux due to pressure and \mathcal{F}_ν the flux due to viscosity. They are defined explicitly as

$$\mathcal{F}_U(x) = \frac{1}{2(2\pi H)^2} \left\langle \int_{x=X} u_x |\mathbf{u}|^2 dy dz - \int_{x=-X} u_x |\mathbf{u}|^2 dy dz \right\rangle_T, \quad (2.13)$$

$$\mathcal{F}_P(x) = \frac{1}{(2\pi H)^2} \left\langle \int_{x=X} u_x P dy dz - \int_{x=-X} u_x P dy dz \right\rangle_T \quad (2.14)$$

$$\mathcal{F}_\nu(x) = \frac{\nu}{(2\pi H)^2} \left\langle \int_{x=-X} u_i \partial_i u_x + u_i \partial_x u_i dy dz - \int_{x=X} u_i \partial_i u_x + u_i \partial_x u_i dy dz \right\rangle_T \quad (2.15)$$

where the integrals are taken at the two planes $x = \pm X$ and summation over the index i is assumed in the last one.

2.3. Energy spectra and fluxes in scale space

The fluxes above describe how energy is transported in physical space. At the same time, energy is also transferred in scale space from large to small scales. To quantify the energy distribution and fluxes in scale space we use the Fourier transformed fields $\tilde{\mathbf{u}}_{\mathbf{k}}(t)$ defined by

$$\tilde{\mathbf{u}}_{\mathbf{k}}(t) = \langle \mathbf{u}(t, \mathbf{x}) e^{-i\mathbf{k} \cdot \mathbf{x}} \rangle_\nu \quad \text{and} \quad \mathbf{u}(t, \mathbf{x}) = \sum_{\mathbf{k}} \tilde{\mathbf{u}}_{\mathbf{k}}(t) e^{i\mathbf{k} \cdot \mathbf{x}}, \quad (2.16)$$

where the inverse wavenumber k^{-1} gives a natural definition of a scale. The energy spectrum, giving the distribution of energy among scales is defined as

$$\tilde{E}(k) = \frac{1}{2} \sum_{k < |\mathbf{q}| < k+1} \langle |\tilde{\mathbf{u}}_{\mathbf{q}}|^2 \rangle_T \quad (2.17)$$

The energy flux gives the rate that energy flows across k is defined as

$$\Pi(k) = - \left\langle \langle \mathbf{u}_k^< \cdot \mathbf{u} \cdot \nabla \mathbf{u} \rangle_\nu \right\rangle_T \quad (2.18)$$

where $\mathbf{u}_k^<$ stands for the velocity field filtered so that only wavenumbers with norm $|\mathbf{k}| < k$ are kept (Alexakis & Biferale 2018; Frisch 1995).

2.4. Reynolds numbers

The Reynolds number in this system provides a measure of the strength of turbulence is typically defined as $Re = U\ell/\nu$ where U is the typical velocity of the system. In this work we are interested in the long box limit $L \gg H$ and some care needs to be taken in order to be able to compare with homogeneous turbulence results. If we define U based on the mean energy density \mathcal{E}_0 (given in eq. 2.3) then if turbulence remains localized, \mathcal{E}_0 will approach zero in the limit $L \gg H$. Thus defining U as the root mean square (rms) value over the entire domain $U = (2\mathcal{E}_0)^{1/2}$ will greatly underestimate the value of U close to the forcing region. The same holds for the mean dissipation rate density \mathcal{D}_0 . To compensate for that we will define the typical velocity U and the typical dissipation rate ϵ as

$$U = \sqrt{\frac{2\mathcal{E}_0 L}{H}}, \quad \epsilon = \mathcal{D}_0 \frac{L}{H} \quad (2.19)$$

The factor L/H introduced makes U and ϵ remain finite in the $L/H \rightarrow \infty$ limit for localised turbulence. These definitions can be interpreted as the rms velocity and dissipation around the forcing region. With these definitions of U and ϵ the following three Reynolds numbers

$N_x \times N_y \times N_z$	Re_ϵ	Re_U	Re_λ
$64 \times 64 \times 512$	2.0	1.7	2.2
$64 \times 64 \times 512$	4.0	4.5	5.8
$64 \times 64 \times 512$	10.0	15.1	16.8
$64 \times 64 \times 512$	20.0	34.7	31.3
$64 \times 64 \times 512$	40.0	78.1	54.1
$128 \times 128 \times 1024$	110	217	92.1
$256 \times 256 \times 2048$	230	502	161
$512 \times 512 \times 4096$	500	1165	270
$1024 \times 1024 \times 8192$	1250	2990	447

Table 1: Resolution and values of the Reynolds numbers $Re_U, Re_\epsilon, Re_\lambda$ achieved in the numerical simulations.

typically met in the literature are defined:

$$Re_U \equiv \frac{UH}{\nu}, \quad Re_\epsilon \equiv \frac{\epsilon^{1/3} H^{4/3}}{\nu}, \quad Re_\lambda \equiv \frac{\sqrt{5}U^2}{(\nu\epsilon)^{1/2}}. \quad (2.20)$$

The first one is the classical definition of the Reynolds number based of the (re-scaled) rms velocity. The second is a Reynolds number based on the energy injection/dissipation and is the one we control in these simulations (since it is the energy injection rate we impose). Finally the third one is the Taylor-Reynolds number based on the Taylor micro scale $\lambda = U\sqrt{5\nu/\epsilon}$. The three definitions are related by

$$5Re_U^4 = Re_\lambda^2 Re_\epsilon^3. \quad (2.21)$$

and for large Re_U it is expected that $Re_U \propto Re_\epsilon \propto Re_\lambda^2$.

2.5. Numerical Setup

The Navier-Stokes equations are solved using the pseudo-spectral code `GHOST` (Mininni *et al.* 2011), that uses a 2/3 de-aliasing rule and a second order Runge-Kuta method for the time advancement. A uniform grid was used such that the grid spacing $\Delta x = 2\pi L/N_x$, $\Delta y = 2\pi H/N_y$ and $\Delta z = 2\pi H/N_z$ are equal where N_x, N_y, N_z is the number of grid points in each direction, with $N_x = 8N_y = 8N_z$.

The simulations were started from the $\mathbf{u} = 0$ initial conditions and continued until a steady state is reached for which a clear mean energy profile can be calculated. The only exception to this rule is the highest resolution run $N_x = 8192$ for which the results of the $N_x = 4096$ run were extrapolated to a larger grid and used as initial conditions. This run was performed for eight turn-over times that was enough to converge sign-definite quantities (like energy) but not sign-indefinite quantities (like fluxes). A list with the properties of all runs performed are given in table 1.

3. Results

We begin with the top panel of figure 2 that shows the energy density $E(t, X)$ for $Re_\epsilon = 500$ for different times. The black dashed line shows the forcing profile that is limited to $|X|/(2\pi H) \lesssim 1/2$. Energy spreads away from the forcing region but at late times it fluctuates around a mean profile shown by the red line. Thus already at this stage it can be testified that energy does not spread in the entire box and it remains close to the forcing region. This

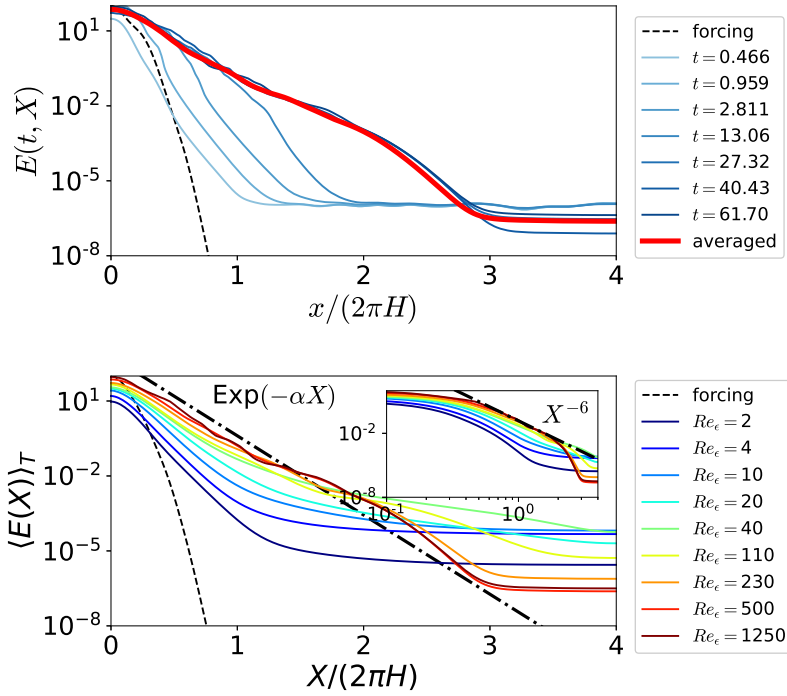


Figure 2: Top panel: The energy density $E(t, X)$ for different times. Bottom panel: The time averaged energy density $\langle E(X) \rangle_T$ at steady state for different values of Re_ϵ in the entire domain, the dashed line indicates the forcing amplitude as a function of X . The inset shows the same data in log-log scale. The same color index is used to mark Re_ϵ in all subsequent figures.

mean profile is shown in the bottom panel of the same figure for different values of Re_ϵ . The different colors indicate the different values of the Reynolds number achieved as marked in the legend. The same colors are used for all subsequent figures. The peak of the local energy density lies close to the forcing region and decays fast away from it. The energy far away from the forcing at $|X|/(2\pi H) \simeq 4$ remains very small such that $E(8\pi H)/E(0) \lesssim 10^{-6}$. In the remaining of this section we will try unravel the processes of this localisation and the implications for the system behavior.

Before continuing with spatial properties of our flow we perform some standard benchmark analysis often used in homogeneous turbulence. Figure 3 shows the scaling of global measures as a function of the Reynolds number. The left panel shows the relation between the different Reynolds numbers where the scaling $Re_U \propto Re_\epsilon \propto Re_\lambda^2$ that holds for large Re is verified. In right panel of figure 3 we show the non-dimensional dissipation rate (or drag coefficient) C_ϵ defined here as:

$$C_\epsilon = \frac{\epsilon H}{U^3}, \quad (3.1)$$

that expresses the rate energy is dissipated non-dimensionalized by the amplitude of the fluctuations. It is a corner-stone conjecture of homogeneous and isotropic turbulence theory that C_ϵ obtains a finite and Re -independent value at large Re . The present data indicate that at large Re_λ , C_ϵ appears to converge to a Re_λ -independent value but quite slowly. Only the largest values of $Re_\lambda \gtrsim 270$ indicate the possibility that such a plateau is reached with a

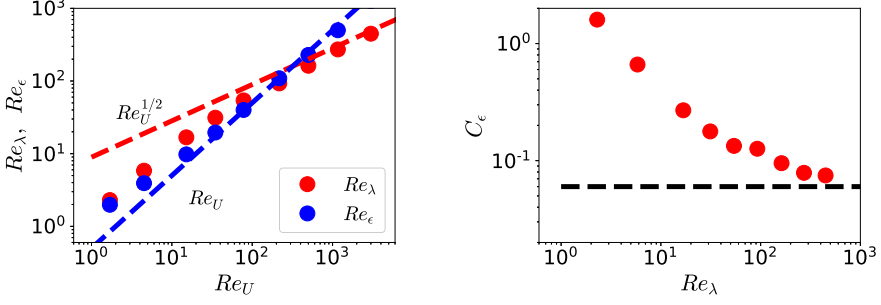


Figure 3: Left: Relation between the different Reynolds numbers $Re_U, Re_\epsilon, Re_\lambda$. Right: The normalized dissipation rate C_f as a function of Re_λ .

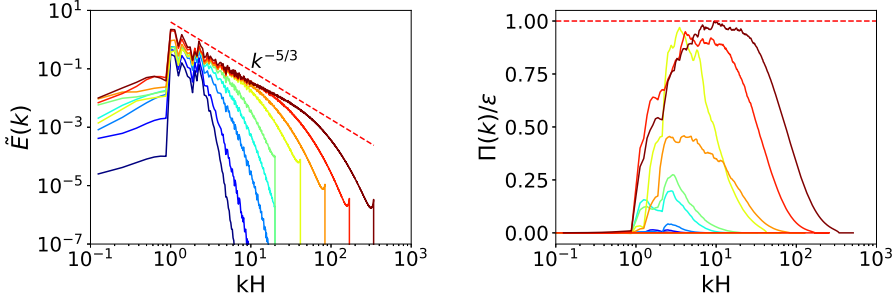


Figure 4: Left: The energy spectra $\tilde{E}(k)$ for the different Re_λ examined. Right: The energy fluxes $\Pi(k)$ for the same runs.

value of $C_\epsilon \simeq 0.06$ that is rather small. In homogeneous and isotropic simulations such a plateau is reached after $Re_\lambda \sim 100$ and at a value much larger $C_\epsilon \simeq 0.5$ (Kaneda *et al.* 2003). This reflects that localized turbulence is affected by the the additional freedom to expand in a larger region suppressing possibly its efficiency to cascade energy to the smaller scales.

Figure 4 examines spectral properties of the flow. In the left panel we plot the energy spectra for the different values of Re . The spectra show similar behavior with homogeneous turbulence flows. As the Reynolds number is increased more scales are excited and a power-law spectrum starts to form with exponent close to the Kolmogorov prediction $\tilde{E}(k) \propto k^{-5/3}$. In the right panel of figure 4 the energy fluxes in Fourier space are plotted. The energy fluxes increase with Re until for the largest Res attained a constant flux range has begun to form. It is worth noting that this constant flux region is obtained at much larger Re than what is observed in homogeneous turbulence simulations reflecting once again a delay in obtaining a Re -independent scaling due to the effect of spreading.

Returning to the spatial properties of the flow and the energy density profile we note that as the Reynolds number is increased the energy increases and also spreads at larger distances. At very large values of Re_λ the energy profile appears to converge to a Re independent profile. This implies that at large Re the energy profile is determined by the self-spreading of eddies due to turbulent advection and not by viscous processes. The fast drop of $E(X)$ can be either an exponential $E(x) \propto \exp(-\alpha x)$ or of fast power law $E(x) \propto |X|^{-6}$ (see inset). The present data can not exclude either option. We point out that since the energy density drops very fast

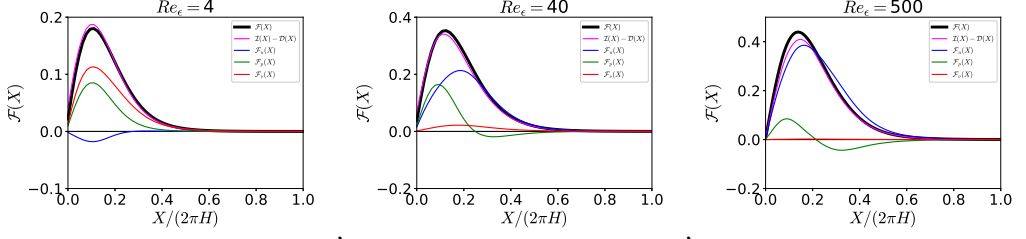


Figure 5: The different energy fluxes in real space as indicated in the legend for three different values of $Re_\epsilon = 4, 40, 500$.

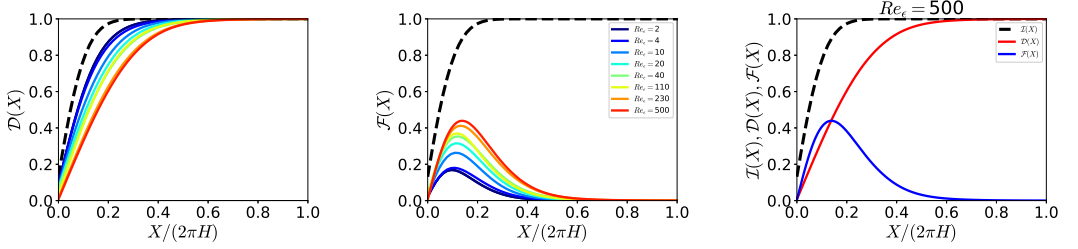


Figure 6: The dissipation rate $\mathcal{D}(X)$ (left panel), the energy flux $\mathcal{F}(X)$ (center panel) for different values of Re . The right panel compares the largest $Re_\epsilon = 500$ for which the fluxes were measured. The dashed line indicates $\mathcal{I}(X)$.

also the local Reynolds number (defined using a local rms velocity) is also decreasing. So it is hard to obtain a large Re behavior in the outer region $|X| \gg H$.

The fact that the energy density reaches a Re -independent profile is not a trivial result. It reflects a balance between the rate energy is transported to larger values of $|x|$ and the rate energy cascades to the small scales. If the cascade process was weaker than the real-space transport then at the $Re \rightarrow \infty$ limit energy would reach the entire domain. On the contrary if the real-space transport was weaker no energy would be found outside the forcing region in the same limit. In other words turbulent diffusion and turbulent dissipation must be of the same order.

To quantify this assertion we look at the fluxes at real space. In figure 5 we plot \mathcal{F}_i for three different values of Re varying from the laminar to the turbulence case. The black line shows the total flux, the blue line the flux due to velocity fluctuations, the green line the flux due to pressure and the red line the flux due to viscosity. The magenta line shows the difference between $\mathcal{I}(x)$ and $\mathcal{D}(x)$. A comparison between the black and magenta lines verifies the relation 2.12. The small differences that are observed are due to insufficient time averaging that is more pronounced in the large resolution runs. A few observations need to follow. For small Re the energy flux is dominated by viscosity with pressure also playing a significant part. The flux due to the velocity fluctuations have a negative sign. As the Reynolds is increased the role of the velocity fluctuations becomes more dominant transferring outwards energy. The transfer due to viscosity diminishes while the transfer due to pressure also takes negative values. At the largest Re almost the entire flux is dominated by the velocity fluctuations with the pressure flux being weaker and positive in the forcing region and negative away from it.

Finally to compare the two dominant processes away from the forcing region the turbulent dissipation and the turbulent diffusion we plot in figure 6 the dissipation rate $\mathcal{D}(X)$ in the

left panel and the total flux $\mathcal{F}(X)$ on the center panels for all Re . The right panel compares the two, for the largest value of Re for which the fluxes were calculated $Re_\epsilon = 500$. The black dashed lines indicates $\mathcal{I}(X)$ that is the same for all Re . As the Reynolds is increased the dissipation is decreased while the flux is increased. For the largest Re at the peak of the flux around $X \simeq 0.15(2\pi H)$ the two processes become of approximately equal marking that the two processes turbulent dissipation and the turbulent diffusion are of the same order.

4. Conclusions

The present work has demonstrated that locally forced turbulence will not spread throughout the domain provided that there is no mean injection of linear or angular momentum. It will remain localised forming an energy density profile that is Re independent in the large Re limit. Away from the forcing region the two dominant effects are turbulent dissipation and turbulent diffusion that were found to be of the same order. The exact functional form of the energy profile could not be determined from the present simulations. Theoretical investigations and modeling could give further insight to this problem.

To expand the understanding of the two involved processes, turbulent diffusion and turbulent dissipation, a simultaneous scale-space and real-space analysis would be required either by introducing local smoothing (Germano 1992; Aluie & Eyink 2009; Eyink & Aluie 2009; Alexakis & Chibbaro 2020) or two point analysis and the Kármán–Howarth–Monin–Hill (KMHM) equation (Hill 2001, 2002). The latter has been used recently to study boundary driven flows (Apostolidis *et al.* 2022, 2023) and wakes Chen & Vassilicos (2022); Chen *et al.* (2021) where the role the inhomogeneous energy injection from the mean flow was emphasised. In the present flow, there is no mean flow and the primary terms in balance are the inter-scale transfer rate and turbulent transport in physical space, both of which are forcing and viscosity independent. Thus a new state of turbulence is present where two inertial effects, the energy flux in scale space and in real space, compete. The fact that these two dominant processes are viscosity-independent makes their modeling particular difficult as there is no simplifying limit where one term will dominate over the other. Careful parametrization would be required so that the correct energy profile is captured.

Finally we would like to add that the present study was limited to a triple periodic channel flow limiting the spreading in only one direction. Its extension to larger domains where turbulence can spread in two or in all three directions is far from trivial and would need to be examined separately. Here experimental investigations would become much more beneficial than numerical simulations.

Funding. This work was granted access to the HPC resources of GENCI-TGCC & GENCI-CINES (Project No. A0130506421). This work has also been supported by the Agence nationale de la recherche (ANR DYSTURB project No. ANR-17-CE30-0004).

Declaration of Interests. The authors report no conflict of interest.

REFERENCES

- ALEXAKIS, ALEXANDROS & BIFERALE, LUCA 2018 Cascades and transitions in turbulent flows. *Physics Reports* **767**, 1–101.
- ALEXAKIS, ALEXANDROS & CHIBBARO, SERGIO 2020 Local energy flux of turbulent flows. *Physical Review Fluids* **5** (9), 094604.
- ALUIE, HUSSEIN & EYINK, GREGORY L 2009 Localness of energy cascade in hydrodynamic turbulence. ii. sharp spectral filter. *Physics of Fluids* **21** (11).
- ALVES-PORTELA, F, PAPADAKIS, G & VASSILICOS, JC 2020 The role of coherent structures and inhomogeneity in near-field interscale turbulent energy transfers. *Journal of Fluid Mechanics* **896**, A16.

- APOSTOLIDIS, ARGYRIOS, LAVAL, JEAN-PHILIPPE & VASSILICOS, JC 2022 Scalings of turbulence dissipation in space and time for turbulent channel flow. *Journal of Fluid Mechanics* **946**, A41.
- APOSTOLIDIS, ARGYRIOS, LAVAL, JEAN-PHILIPPE & VASSILICOS, JC 2023 Turbulent cascade in fully developed turbulent channel flow. *To appear in Journal of Fluid Mechanics*.
- ARAKI, RYO & BOS, WOUTER JT 2022 Inertial range scaling of inhomogeneous turbulence. *arXiv preprint arXiv:2210.14516*.
- BALL, CG, FELLOUAH, H & POLLARD, A 2012 The flow field in turbulent round free jets. *Progress in Aerospace Sciences* **50**, 1–26.
- BERTI, S, BOFFETTA, G & MUSACCHIO, S 2023 Mean flow and fluctuations in the three-dimensional turbulent cellular flow. *Physical Review Fluids* **8** (5), 054601.
- CAFIERO, GIOACCHINO & VASSILICOS, JC 2019 Non-equilibrium turbulence scalings and self-similarity in turbulent planar jets. *Proceedings of the Royal Society A* **475** (2225), 20190038.
- CARAZZO, GUILLAUME, KAMINSKI, EDOUARD & TAIT, STEPHEN 2006 The route to self-similarity in turbulent jets and plumes. *Journal of Fluid Mechanics* **547**, 137–148.
- CHEN, JG, CUVIER, C, FOUCAUT, J-M, OSTOVAN, Y & VASSILICOS, JC 2021 A turbulence dissipation inhomogeneity scaling in the wake of two side-by-side square prisms. *Journal of Fluid Mechanics* **924**, A4.
- CHEN, JG & VASSILICOS, JOHN CHRISTOS 2022 Scalings of scale-by-scale turbulence energy in non-homogeneous turbulence. *Journal of Fluid Mechanics* **938**, A7.
- CIMARELLI, ANDREA, DE ANGELIS, ELISABETTA, JIMENEZ, JAVIER & CASCIOLA, CARLO MASSIMO 2016 Cascades and wall-normal fluxes in turbulent channel flows. *Journal of Fluid Mechanics* **796**, 417–436.
- EYINK, GREGORY L & ALUIE, HUSSEIN 2009 Localness of energy cascade in hydrodynamic turbulence. i. smooth coarse graining. *Physics of Fluids* **21** (11).
- FRISCH, URIEL 1995 *Turbulence: the legacy of AN Kolmogorov*. Cambridge university press.
- GERMANO, MASSIMO 1992 Turbulence: the filtering approach. *Journal of Fluid Mechanics* **238**, 325–336.
- GOMES-FERNANDES, R, GANAPATHISUBRAMANI, B & VASSILICOS, JC 2015 The energy cascade in near-field non-homogeneous non-isotropic turbulence. *Journal of Fluid Mechanics* **771**, 676–705.
- HILL, REGINALD J 2001 Equations relating structure functions of all orders. *Journal of Fluid Mechanics* **434**, 379–388.
- HILL, REGINALD J 2002 Exact second-order structure-function relationships. *Journal of Fluid Mechanics* **468**, 317–326.
- JIMÉNEZ, JAVIER 2012 Cascades in wall-bounded turbulence. *Annual review of fluid mechanics* **44**, 27–45.
- KANEDA, YUKIO, ISHIHARA, TAKASHI, YOKOKAWA, MITSUO, ITAKURA, KEN'ICHI & UNO, ATSUYA 2003 Energy dissipation rate and energy spectrum in high resolution direct numerical simulations of turbulence in a periodic box. *Physics of Fluids* **15** (2), L21–L24.
- LANDAU, LEV DAVIDOVICH & LIFSHITZ, EVGENII MIKHAILOVICH 2013 *Fluid Mechanics: Landau and Lifshitz: Course of Theoretical Physics, Volume 6*, , vol. 6. Elsevier.
- LIST, EJ 1982 Turbulent jets and plumes. *Annual review of fluid mechanics* **14** (1), 189–212.
- MININNI, PABLO D, ROSENBERG, DUANE, REDDY, RAGHU & POUQUET, ANNICK 2011 A hybrid mpi–openmp scheme for scalable parallel pseudospectral computations for fluid turbulence. *Parallel computing* **37** (6-7), 316–326.
- MOLLICONE, J-P, BATTISTA, F, GUALTIERI, P & CASCIOLA, CM 2018 Turbulence dynamics in separated flows: the generalised kolmogorov equation for inhomogeneous anisotropic conditions. *Journal of Fluid Mechanics* **841**, 1012–1039.
- VALENTE, PC & VASSILICOS, JOHN CHRISTOS 2011 The decay of turbulence generated by a class of multiscale grids. *Journal of Fluid Mechanics* **687**, 300–340.